

FUSELAGE AERODYNAMIC DRAG PREDICTION METHOD BY CFD

Fabrizio Nicolosi

University of Naples Federico II

Associate Professor

Via Claudio 21, 80125, Naples,

fabrizio.nicolosi@unina.it

Pierluigi Della Vecchia (University of Naples Federico II, Post-Doc, Via Claudio 21, 80125, Naples,

pierluigi.dellavecchia@unina.it),

Daniilo Ciliberti (University of Naples Federico II, PhD Student, Via Claudio 21, 80125,

Naples, daniilo.ciliberti@unina.it),

Vincenzo Cusati (University of Naples Federico II, Consultant, Via Claudio 21, 80125,

Naples, vincenzo.cusati@gmail.com.)

ABSTRACT

The aim of this work is the development of a new methodology to predict fuselage aerodynamic drag through CFD aerodynamic calculations. The investigation has been focused on typical large turboprop fuselage geometry. The geometry has been divided into three main components: nose, cabin, and fuselage tail. Fuselage fineness ratio, windshield angle (Ψ), and upsweep angle (θ), have been used as independent (geometric) variables to derive the drag prediction methodology. These parameters have been varied one by one, keeping the others constant. Several fuselage geometries have been generated and then analysed with Star-CCM+ in viscous, compressible flow regime. The effect of a high-wing-fuselage fairing has been also evaluated in terms of fuselage drag, varying the length and the fairing height. Results present a simple method to estimate the isolated fuselage drag coefficient and to take into account for a high-wing fairing geometry, typical for a turboprop aircraft.

1 INTRODUCTION

This paper presents new preliminary design methodologies to estimate the drag aerodynamic coefficient of transport large turbopropeller aircraft fuselage. Method has been developed by numerical aerodynamic analyses performed with STAR-CCM+[®] (Ref. [1]) and it has been focused on the estimation of aerodynamic drag coefficients. Similar numerical approach to develop a methodology to be applied in preliminary design phase has been already carried out by the authors, which have deeply investigated the aerodynamics of the vertical tailplane and the aerodynamic interference among airplane components caused by rudder deflection [2]. The result of these studies is a methodology which effectiveness is not enclosed only for the turboprop air transport category, but it has also been exploited for the preliminary design of a new general aviation commuter aircraft [4].

The aerodynamic design of the fuselage of a transport aircraft is a crucial item in airplane preliminary design. About 30% of zero lift drag is due to the fuselage [8]. Aircraft cruise performance, such as maximum flight speed or fuel consumption, are mainly dependent from the zero lift drag coefficient and they could be improved with a more accurate aerodynamic design. Moreover aircraft longitudinal and directional stability characteristics are strictly related to the fuselage contribution, thus an accurate estimation of the latter could lead to a better tailplane design and aircraft stability characteristics.

Aircraft preliminary design usually relies on semi-empirical methodologies, based on heritage aircraft geometries and wind tunnel tests conducted mainly by NACA [9]. Semi-empirical methods consider the drag coefficient as the sum of different contributions that can be evaluated by relations obtained from wind tunnel test data, most of which are collected in the USAF DATCOM database [14]. The total drag coefficient of an aircraft can be expressed as the sum of the zero lift drag coefficient and the drag-due-

to-lift coefficient. This assumption is valid when the approximation of a parabolic drag polar is used in order to estimate the drag coefficient for low incidence such as cruise and climb, that is until the lift coefficient becomes greater than 1. The zero lift drag coefficient is also known as parasite drag coefficient and it includes skin friction (function of wetted area), windshield effect angle ψ , upsweep effect angle θ , and base drag contributions [14].

Researchers at University of Naples have been working on the development of design techniques for light and general aviation aircraft since 1996 [19]. Application of such developed or matured methodologies for aerodynamic design have been previously shown in [20]. The matured experience have been also applied through deep investigation on the aerodynamic effects of wing tip and boundary layer control on aircraft performance [21]. The matured know-how in aircraft aerodynamic design have been also linked to some validation obtained through dedicated flight test activity [23].

Section 2 shows the fuselage geometries involved in this paper, Section 3 describes the set-up of the computational domains and the fluid physic. Section 4 illustrates the drag prediction method and the fairing effects on the drag coefficient and in section 5 conclusions are addressed.

2 FUSELAGE GEOMETRIES

A modular model of a 80-seats fuselage of a generic regional turboprop aircraft has been considered as reference layout, which leads to a fuselage length of about 30 m and a fuselage diameter of 3.4 m. This geometry has a fineness ratio of about 9 and it has been divided into three main components: nose, cabin, and tailcone (see Figure 1). For each component, main geometrical parameters have been defined as shown in Figure 1, Figure 2 and summarized in Table 1. The ratio of the fuselage length and diameter is the fineness ratio FR , whereas the ratio between the nose length and diameter and tailcone length and the diameter are respectively the fineness ratio of the nose FR_n and of the tail FR_t . In order to define the windshield (ψ) and upsweep (θ) angles, the h_w and h_u parameters have been introduced. The first locates the height of the intersection point between the horizontal line and the tangent to nose contour. The latter locates the height of the intersection point between the horizontal line and the tangent to tail contour. Both are defined in Table 1.

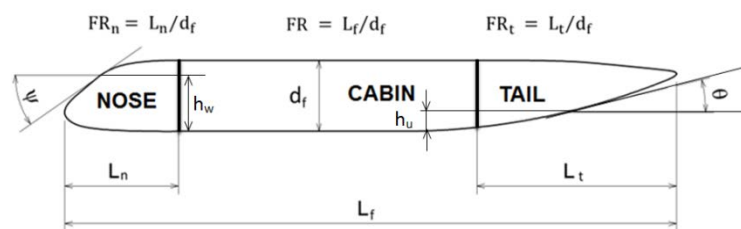


Figure 1 Main fuselage geometrical parameters.

Table 1 Definition of geometrical parameters.

L_f	d_f	L_n	L_c	L_t	FR	FR_n	FR_t	h_w/d_f	h_u/d_f	ψ	θ
30 m	3.4 m	5.7 m	13 m	11.3 m	8.7	1.6	2.8	0.75	0.26	40°	14°

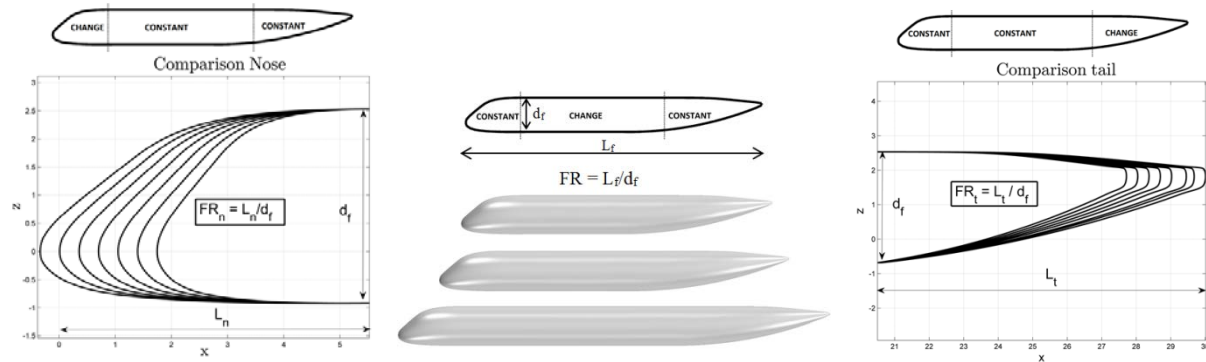


Figure 2 Fineness ratio variations, fuselage nose (left), fuselage cabin (middle), fuselage tail (right).

2.1 Wing-Fuselage fairing

In order to estimate the wing-fuselage fairing effect on fuselage drag coefficient, a simple straight-tapered high wing geometry has been considered, joined to the fuselage with a fairing geometry as suggested in [8] by the authors. This geometry can be ideally divided into two main parts: the forward part which has a length of 8% of L_f , and an aft part which has a length of about 6% L_f . Starting from a reference fairing geometry shown in Figure 3, the latter has been modified by an isomorphism in length and height (see Figure 3).

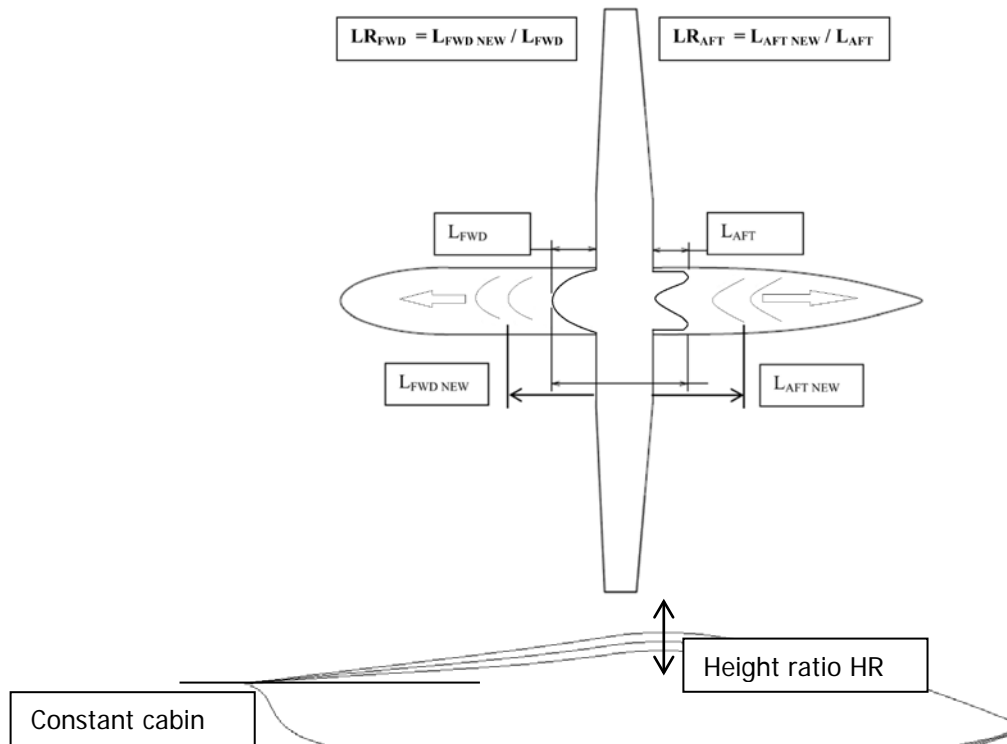


Figure 3 Wing-fuselage fairing design parameters.

This figure also shows the parameters used to define the *stretching ratio* of the wing-fuselage fairing. For both the forward and the aft parts, the stretching factor is defined as the ratio of the length of the modified geometry to the length of the baseline geometry (LR_{FWD} , LR_{AFT}). The modifications in height are expressed with respect to the reference height which is equal to 2% L_f measured from the fuselage constant cabin.

3 MESH AND PHISICS SET-UP

The models investigated in this work are the fuselage of a large regional transport turboprop aircraft and the wing-fuselage with a fairing geometry. The numerical domain is a typical parallelepiped domain with model located on the longitudinal plane of symmetry, at one third of the block length from the inlet face (see Figure 4). Polyhedral mesh (built into STAR-CCM+® [1]) has been used with 20 prismatic layers to better predict the boundary layer phenomena. Viscous compressible RANS equations have been solved with Spalart-Allmaras turbulent model. Mesh independency and solution convergence have been monitored by looking equations residuals (around to 10^{-7}), aerodynamic coefficients stabilization and $y^+ \approx 1$ value varying the number of cells (see Figure 5). Isolated fuselage aerodynamic analyses have been performed with a mesh of about 2.3 millions of cells for fuselage semi-model and 6.4 millions of cells for the wing-body-fairing configuration.

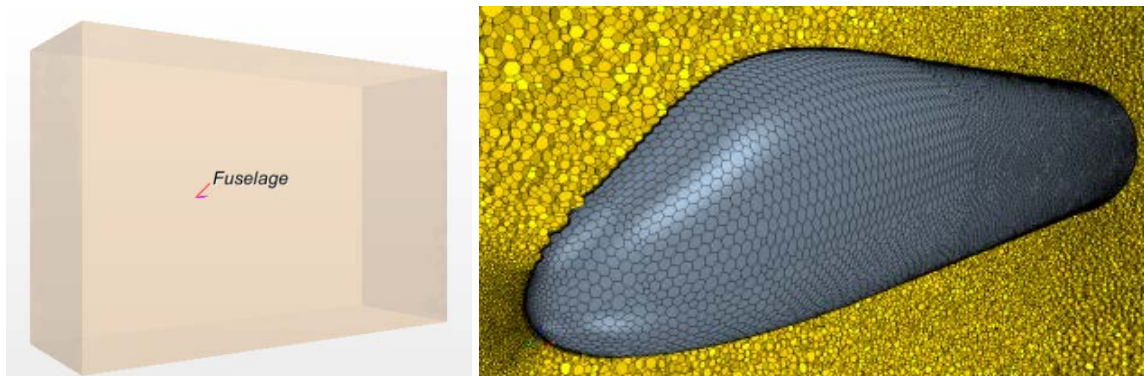


Figure 4 Computational domain and polyhedral volume mesh.

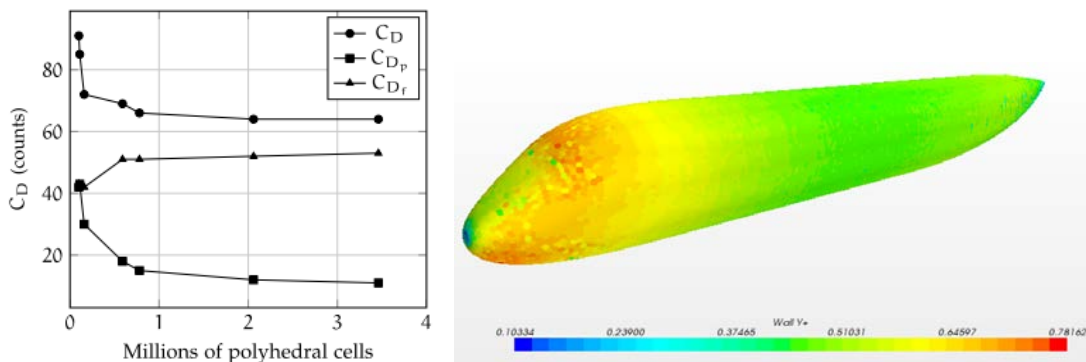


Figure 5 Fuselage Drag coefficient vs number of cells and wall y^+ .

All the aerodynamic analyses have been performed at typical cruise flight condition with a Mach number equal to 0.52 and a Reynolds number (based on the fuselage length) of 2.0×10^8 at zero degrees of angle

of attack ($\alpha=0$ deg., $M=0.52$, $Re=2.0 \times 10^8$). In order to evaluate the wing fuselage fairing effect in a wide range of angle of attack, a typical climb condition has been also investigated ($\alpha=8$ deg., $M=0.23$, $Re=1.5 \times 10^8$). All the mesh and physics set-up data are summarized in Table 2.

Table 2 Mesh and physics settings.

Mesh data	
Mesh Type	Polyhedral cells
Base size	12.0 m
Farfield dimensions	30 L_f 10 L_f 20 L_f
Number of prism layers	20
Prism layer stretching	1.3
Number of cells	2380515 fuselage 6423155 wing-fuselage-fairing
Min. cell size	0.1% base size
Target cell size	1% base size
Prism layer size	0.03% base size
Physics data	
Angle of attack	0 – 8 degrees
Reynolds Number	$2.02 \cdot 10^8$ (based on L_f) $1.50 \cdot 10^8$ (based on L_f)
Mach Number	0.52 0.23

4 DRAG PREDICTION METHOD

The method allows computing the fuselage drag coefficient as the sum of the contributions of each component (nose, cabin, and tailcone). This approach does not allow evaluating some sources of drag as leakage, wiper, surface roughness, and excrescences. The hypothesis of the super-positioning of the effects has been verified, since the geometry modifications of one part of the fuselage affect only the drag coefficient of that part [18].

$$C_{D_{fus}} = \left(K_n \frac{S_{wetnose}}{S_{wet}} + K_c \frac{S_{wetcabin}}{S_{wet}} + K_t \frac{S_{wettail}}{S_{wet}} \right) C_{D_{fp}} \frac{S_{wet}}{S_{front}} \quad (1)$$

where definitions of the main parameters present in the Eq. (1) are:

- $C_{D_{fus}}$ is the drag coefficient of the fuselage referred to S_{front} .
- K_n is the nose shape factor. It depends on windshield angle, ψ , and on the FR_n (see Sec. 4.1).
- K_c is the cabin shape factor. It depends on the FR (see Sec. 4.2).
- K_t is the tailcone shape factor. It depends on upsweep angle, θ , and on the FR_t (see Sec. 4.3).

- C_{Dfp} is the drag coefficient of the equivalent flat plate and it coincides with the skin friction coefficient, which can be computed from the following Eq. (2).

$$C_{Dfp} = \frac{0.455}{(\text{Log Re})^{2.58} \cdot (1 + 0.144M^2)^{0.58}} \quad (2)$$

4.1 Fuselage nose factor

The nose shape factor K_n represents the contribution of the nose to the global drag coefficient and it takes into account the effect of the nose fineness ratio and of the windshield geometric angle ψ . It is defined in Eq. (3). In Figure 6 the curves of K_n are drawn as a function of FR_n and parameterized with ψ (windshield angle).

$$K_n = \frac{C_{Dn} S_{\text{front}}}{C_{Dfp} S_{\text{wetnose}}} \quad (3)$$

These curves have been obtained from numerical results. For each numerical simulation, the value of C_{Dn} (which is the value of the drag coefficient estimated only on the nose surface and it is referred to S_{front}) has been calculated, along the value of the equivalent skin friction coefficient C_{Dfp} by Eq. (2), and the wet surfaces for each component been accounted for, then the K_n curves have been generated with Eq. (3). The end-user does not have to use the equation to calculate the K_n factor, but he only has to refer to the chart.

As it can be seen in Figure 6, the K_n factor decreases as FR_n increases and ψ angle decreases, meaning that the fuselage drag coefficient decreases.

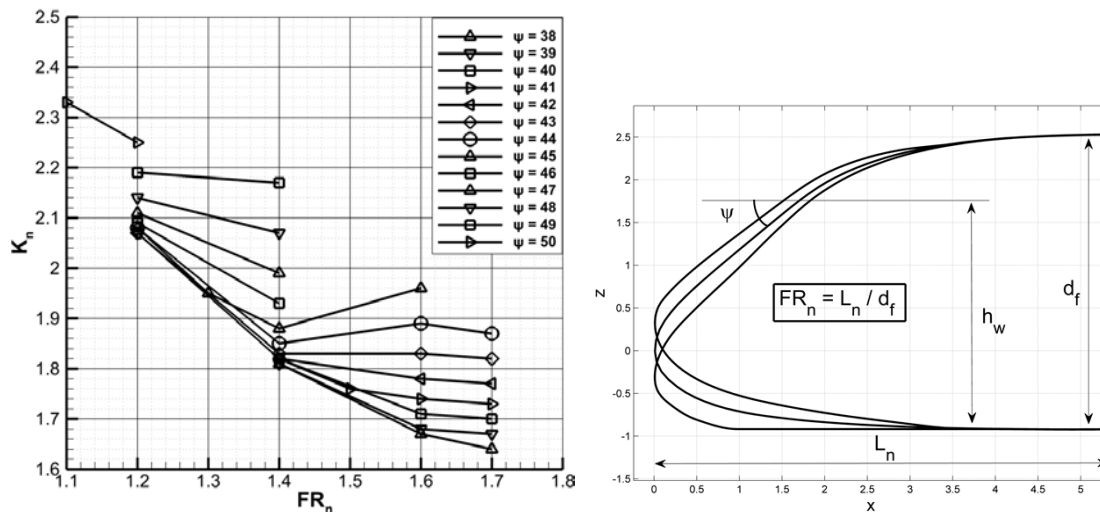


Figure 6 Nose shape factor as a function of nose fineness ratio, $\alpha = 0$ deg.

4.2 Fuselage cabin factor

The fuselage shape factor K_c represents the contribution of the cabin to the global drag coefficient and it takes into account the effect of the cabin length (or cabin fineness ratio). It is important to notice that fuselage FR is primarily dependent from cabin FR . It is defined in Eq. (4). In Figure 7 the curve of K_c is

drawn as a function of FR . As for the nose shape factor, this curve must be used to get the value of the shape factor in order to apply the method. Again, the end-user of the method has to refer to the chart only, whereas the equation states how the K_c curves have been generated from the results of numerical analyses. Figure 7 shows that K_c factor decreases with the fuselage fineness ratio up to $FR \approx 10$ and it tends to be constant for higher FR values. This fact implies that it is not useful to increase the fuselage cabin (and so FR) over $FR=9-10$ because of an increment in wetted surface and hence an increment in parasite drag coefficient (see also Eq. (1)).

$$K_c = \frac{C_{Dc} S_{\text{front}}}{C_{Dfp} S_{\text{wetcabin}}} \quad (4)$$

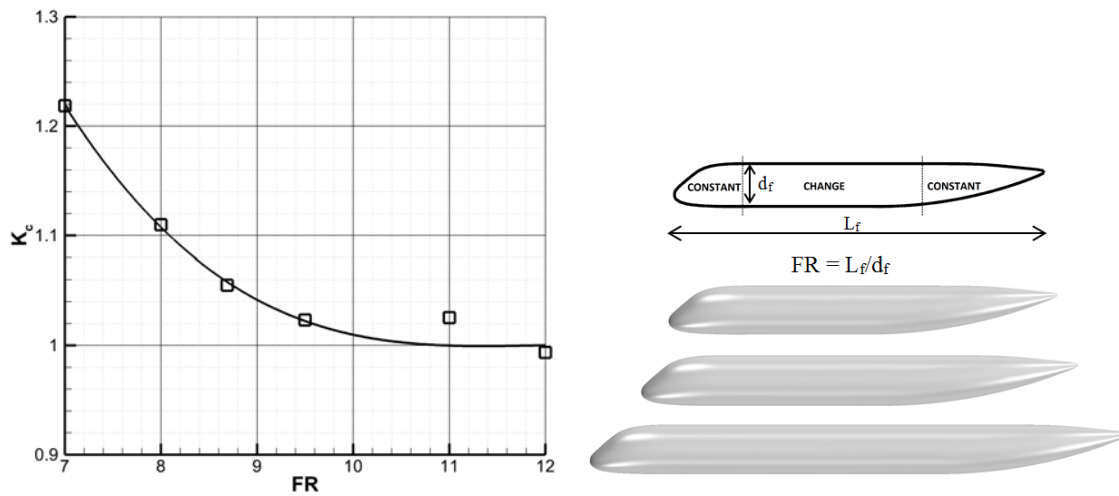


Figure 7 Cabin shape factor as a function of fineness ratio, $\alpha = 0$ deg.

4.3 Fuselage tailcone factor

The tail shape factor K_t represents the contribution of the tail to the global drag coefficient and it takes into account the effect of the upsweep angle θ . It has been estimated from the CFD value of the coefficient C_{Dt} (value of the drag coefficient estimated only on the tail surface) which is referred to S_{front} . In the same chart, the curve of θ_{max} is traced. This curve is the locus of the maximum possible value of the upsweep angle for a fixed fineness ratio. The following equation states how the K_t curves have been calculated.

$$K_t = \frac{C_{Dt} S_{\text{front}}}{C_{Dfp} S_{\text{wettail}}} \quad (5)$$

In Figure 8 the curves of K_t are drawn as a function of FR_t and parameterized in θ . As for the other shape factors, these curves must be used to get the value of the tailcone shape factor in order to apply the method. For a given upsweep angle (see Figure 8), the longer is the tail, the bigger is the drag coefficient. This is due to the increased wetted area. Conversely, for a given tailcone slenderness, the higher is the upsweep angle, the bigger is drag coefficient. In this last case, what is saved in skin friction (wetted area) is lost in pressure drag.

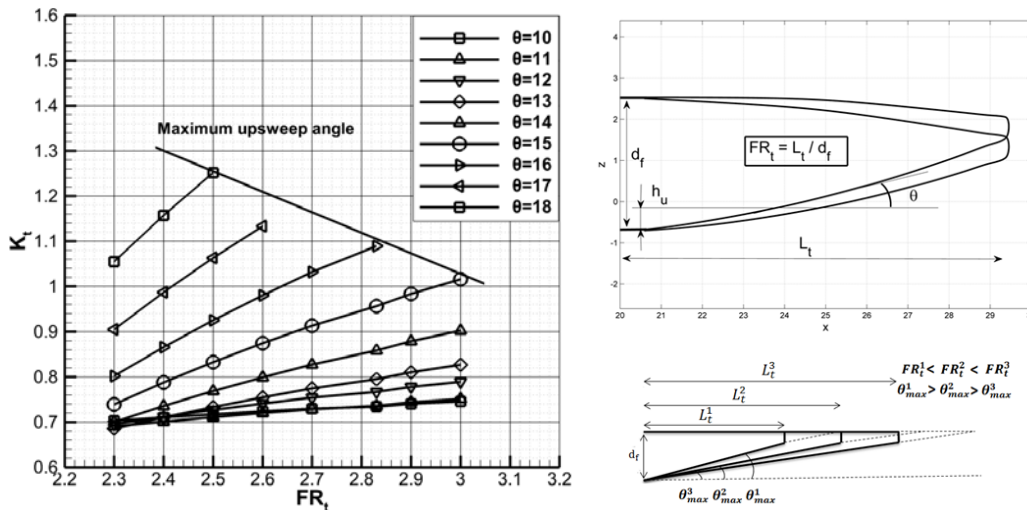


Figure 8 Tail shape factor as a function of tail fineness ratio (FR_t), $\alpha = 0$ deg, and scheme of the geometric relationship between maximum value of upsweep angle (θ) and FR_t .

4.4 Wing-Fuselage fairing effects

Wing-fuselage geometry has been joined with a typical high-wing-fuselage fairing as suggested in Ref. [8] and shown in Figure 3. The reference wing-fuselage-fairing has been lengthened and shortened both forward and aft. The drag coefficient results due to fairing length variation are shown in Figure 9 and for cruise and climb conditions respectively. These charts depict the difference in terms of drag coefficient of the reference geometry and the modified ones, where the abscissa represents the stretching of the rear part and the different curves represent the stretching of the forward part. As it can be seen, lengthening the rear part leads to a drag reduction 4 times (4 drag counts) higher than to the stretching of the forward part (about 1 drag count). This is due to the fact that, on the forward part the flow accelerates with a favorable pressure gradient (after a first deceleration in correspondence of the fuselage-fairing junction). Conversely on the aft part of the fairing-fuselage geometry the flow proceeds with an adverse pressure gradient, slowing down until separation occurs. In climb condition (see Figure 9 right) the effect of lengthening of the fairing rear part is similar to the cruise condition, while the slightly shorter aft panel leads to a higher drag reduction than the reference one (due to the angle of attack). However the drag reduction effect of stretching the aft part is better than the stretching of the forward part (4 times higher). Both cruise and climb conditions of Figure 9 show that for a given fairing forward length, a stretching value $LR_{AFT} \approx 2$ leads to a minimum value for drag coefficient.

Figure 10 shows the effect on drag coefficient of lowering wing-fuselage fairing geometry, for a given forward length ratio $LR_{FWD} = 1.5$ as function of LR_{AFT} . For a given fairing rear part, a 8%, 16% of geometry lowering leads to a drag reduction of about 3, 6 drag counts respectively. This behavior is similar both in cruise and climb condition.

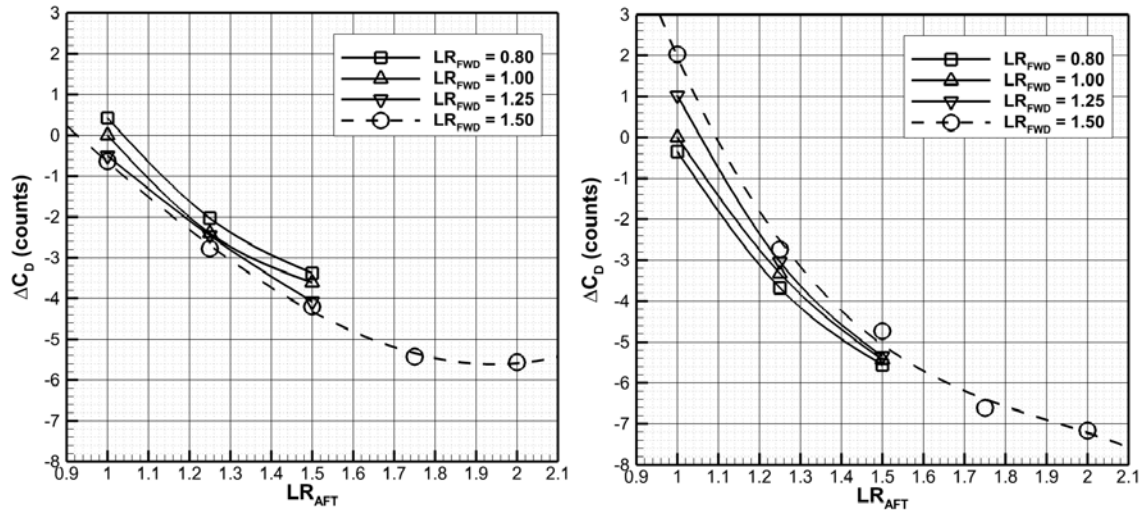


Figure 9 Difference in drag counts with respect to reference wing-fuselage-fairing for the configurations analysed, cruise (left) climb (right).

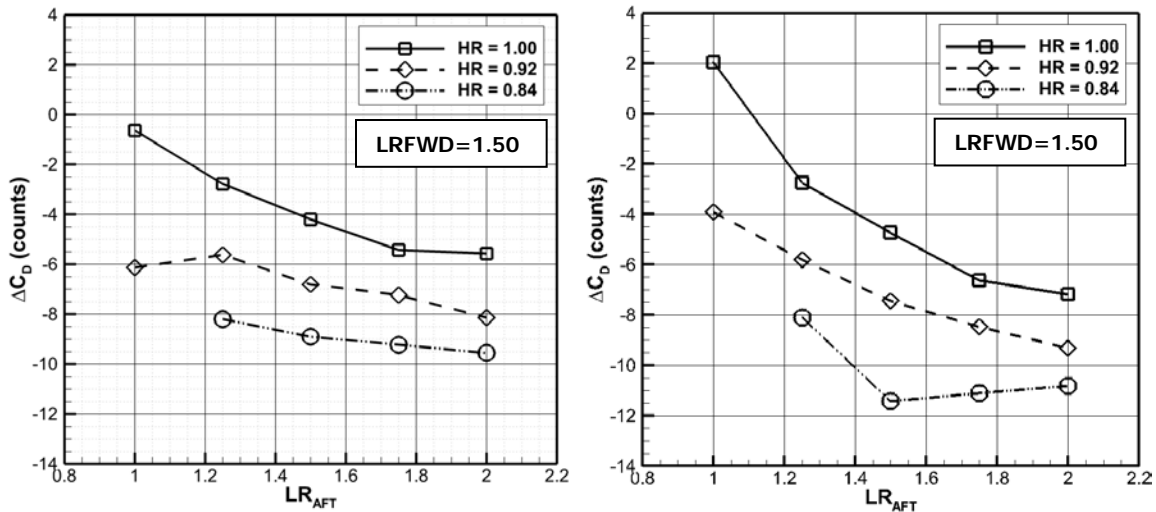


Figure 10 Difference in drag coefficient from the reference wing-fuselage fairing configuration, for both cruise (left) and climb (right) conditions. $LR_{FWD} = 1.50$.

Assuming a wing-fuselage geometry Figure 9 and Figure 10 can be useful in order to preliminary design of a high wing-fuselage fairing geometry. On a typical turboprop aircraft a stretching of the aft part is more suitable than the stretching of the forward part. A good compromise could be a length ratio of the forward part $LR_{FWD}=1.25$ (10% of L_f) and a length ratio of the rear part $LR_{FWD}=1.9$ (11% of L_f). The fairing height should be the lower possible according to configuration.

4.5 Method application

In order to verify the methodology proposed in Section 4, fuselage geometries shown in Figure 11 have been analyzed with STAR-CCM+® (Ref. [1]) and compared with the new proposed method. Results are summarized in Table 3, compared to typical semi-empirical methodology. Results show a very good

agreement between the CFD analyses and the proposed method, especially on test cases 1, 2, and 3, with a difference of about 1 drag count. Test 4 and Test 5 show a drag coefficient difference of 6 and 4 drag counts respectively. This is probably due to windshield and tailcone shapes. It has to be noted that typical semiempirical method (based on skin friction contribution, upsweep, windshield, and base drag) usually overpredicts the drag coefficient respect to the CFD value.

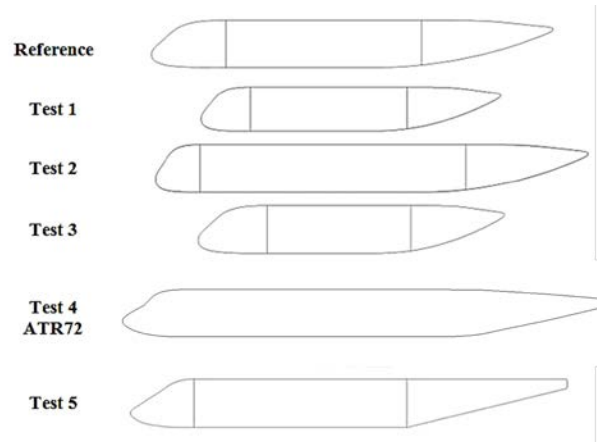


Figure 11 Fuselage geometries used for test cases.

Table 3 Comparison of drag coefficient dimensionless on wing surfaces and on fuselage front surface. The DATCOM values include skin friction, the contributions of upsweep and windshield and the base drag.

	d_f (m)	S_{front} (m ²)	S_w (m ²)	C_D referred to S_{front}			C_D referred to S_w (drag counts)		
				DATCOM	CFD	Method	DATCOM	CFD	Method
Reference	3.45	9.35	75.5	0.0532	0.0472	0.0470	88	78	78
Test 1	3.45	9.35	75.5	0.0509	0.0469	0.0462	84	78	77
Test 2	3.45	9.35	75.5	0.0557	0.0592	0.0595	92	98	99
Test 3	3.45	9.35	75.5	0.0486	0.0449	0.0443	81	74	73
Test 4 (ATR72)	2.63	6.03	61	0.0744	0.0647	0.0599	86	75	69
Test 5	3.15	7.79	75.5	0.0769	0.0627	0.0576	85	79	75

5 CONCLUSIONS

CFD-based fuselage aerodynamic drag prediction method has been addressed. The proposed method is fast to apply and reliable on slender fuselage geometries, also highlighting the effects of geometrical parameters on drag coefficient. It is the authors' opinion that these new methods can be useful in the preliminary design phase of an aircraft. Some applications have shown the effectiveness of the new approach on typical turboprop transport airplane geometries. The effect of a high-wing-fuselage fairing variation on fuselage drag coefficient is presented, useful in the design of this component.

6 REFERENCE

- [1] Star-CCM+, Software Package, Ver. 8.04, CD-adapco, Melville, NY, 2013.
- [2] Nicolosi, F., Della Vecchia, P., Ciliberti, D., "An investigation on vertical tailplane contribution to aircraft sideforce," *Aerospace Science and Technology*, Vol. 28, N. 1, July 2013, pp. 401–416. doi: 10.1016/j.ast.2012.12.006
- [3] Nicolosi, F., Della Vecchia, P., Ciliberti, D., "Aerodynamic interference issues in aircraft directional control," *ASCE's Journal of Aerospace Engineering*, Vol. 28, N. 1, January 2015, ISSN 0893-1321. doi: 10.1061/(ASCE)AS.1943-5525.0000379.
- [4] Nicolosi, F., Della Vecchia, P., Corcione, S., "Design and Aerodynamic Analysis of a Twin-engine Commuter Aircraft," *Aerospace Science and Technology*, Volume 40, January 2015, Pages 1–16. doi: 10.1016/j.ast.2014.10.008.
- [5] Nicolosi F., Della Vecchia P., Corcione S., "Aerodynamic Analysis and Design of a Twin Engine Commuter Aircraft," *ICAS 2012 Proceedings*, Optimage Ltd., UK, September 2012, Vol. 1 pp. 321-332. Proceedings ISBN 978-0-9565333-1-9.
- [6] Nicolosi F., Della Vecchia P., Corcione S., "Commuter Aircraft Aerodynamic Design: Wind-Tunnel tests and CFD Analysis", *ICAS 2014 Proceedings* [CD-ROM], Optimage Ltd., UK, 2014. Proceedings ISBN 3-932182-80-4.
- [7] Nicolosi, F., Corcione, S. and Della Vecchia P., "Commuter Aircraft Aerodynamic Characteristics through Wind Tunnel Tests", *Aircraft Engineering and Aerospace Technology*, ISSN: 0002-2667. doi: 10.1108/AEAT-01-2015-0008.R1.
- [8] Della Vecchia, P., and Nicolosi, F., "Aerodynamic guidelines in the design and optimization of new regional turboprop aircraft," *Aerospace Science and Technology*, Vol. 38, October 2014, pp. 88-104. doi: 10.1016/j.ast.2014.07.018
- [9] Munk, M. M., The Aerodynamic forces on airship hulls, NACA TR-184, 1924.
- [10] Abbott, I. H., Fuselage drag tests in the variable density wind tunnel: streamline bodies of revolution, fineness ratio of 5, NACA TN-614, 1939.
- [11] Gilruth, R. R. and White, M. D., Analysis and prediction of longitudinal stability of airplanes, NACA TR-711, 1941.
- [12] Multhopp, H., Aerodynamics of the fuselage, NACA TM-1036, 1942.
- [13] Draley, E. C., High speed drag test of several fuselage shapes in combination with a wing, NACA WR-L-542, 1947.
- [14] Finck, R. D., "USAF stability and control DATCOM," McDonnell Douglas Corporation, Rept. AFWAL-TR-83-3048, Wright-Patterson Air Force Base, OH, 1978.
- [15] Roskam, J., *Airplane Design Part VI: Preliminary Calculation of Aerodynamic, Thrust and Power Characteristics*, DAR Corporation, Lawrence, KS, 2000.
- [16] Torenbeek, E., *Synthesis of Subsonic Airplane Design*, Delft University Press, Delft, The Netherlands, 1982.
- [17] Perkins, C. D., and Hage, R. E., *Airplane Performance Stability and Control*, Wiley, New York, 1949.
- [18] Nicolosi, F., Della Vecchia, P., Ciliberti, D., and Cusati, V., "Development of new preliminary design methodologies for regional turboprop aircraft by CFD analyses," *ICAS 2014 Proceedings* [CD-ROM], Optimage Ltd., UK, 2014. Proceedings ISBN 3-932182-80-4
- [19] Coiro, D.P., Nicolosi, F. "Design of Low-Speed Aircraft by Numerical and Experimental Techniques Developed at DPA," *Aircraft Design Journal*, Vol. 4, N. 1, Pag1-18, March 2001. ISSN 1369-8869, doi: 10.1016/S1369-8869(00)00020-3.

- [20] Coiro, D.P., Nicolosi, F. Grasso, F. "Design and Testing of Multi-Element Airfoil for Short-Takeoff-and-Landing Ultralight Aircraft," *Journal of Aircraft*, Vol. 46, N. 5, Sept.-Oct. 2009, pp. 1795-1807. ISSN 0021-8669. doi: 10.2514/1.43429.
- [21] Coiro, D. P., Bellobuono, E.F., Nicolosi, F., Donelli, R., "Improving aircraft Endurance through turbulent separation control by pulsed blowing, " *Journal of Aircraft*, Vol. 45, N. 3, May-June 2008, pp. 990-1001. ISSN 0021-8669. doi: 10.2514/1.33268.
- [22] Coiro, D.P., Nicolosi, F., Scherillo, F., Maisto, U. "Improving Hang-Glider Maneuverability using multiple winglets: a numerical and experimental investigation, " *Journal of Aircraft*, Vol. 45, N. 3, May-June 2008, pp. 981-989. ISSN 0021-8669. doi: 10.2514/1.33265
- [23] Nicolosi, F., De Marco, A., Della Vecchia, P., "Flight Tests, Performances and Flight Certification of a Twin-Engine Light Aircraft," *Journal of Aircraft*, Vol. 48, N. 1, January-February 2011, pp. 177-192. ISSN 0021-8669. doi: 10.2514/1.C031056
- [24] Nicolosi, F., De Marco, A., Della Vecchia, P. "Stability, Flying Qualities and Longitudinal Parameter Estimation of a Twin-Engine CS23 Certified Light Aircraft, " *Aerospace Science and Technology (Elsevier)*, Vol. 24, N. 1, January-February 2013, pp. 226-240. ISSN 1270-9638. doi: 10.1016/j.ast.2011.11.011